Article

Exploring Structural Insights of Aβ42 and α-Synuclein Monomers and Heterodimer: A Comparative Study Using Implicit and Explicit Solvent Simulations

Yuliia Varenyk, Panagiotis E. Theodorakis, Dinh Q. H. Pham, Mai Suan Li, and Paweł Krupa*
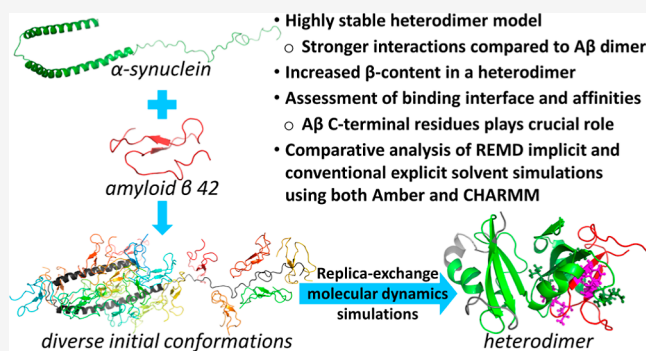
Read Online

ACCESS | Metrics & More | Article Recommendations | Supporting Information

ABSTRACT: Protein misfolding, aggregation, and fibril formation play a central role in the development of severe neurological disorders, including Alzheimer's and Parkinson's diseases. The structural stability of mature fibrils in these diseases is of great importance, as organisms struggle to effectively eliminate amyloid plaques. To address this issue, it is crucial to investigate the early stages of fibril formation when monomers aggregate into small, toxic, and soluble oligomers. However, these structures are inherently disordered, making them challenging to study through experimental approaches. Recently, it has been shown experimentally that amyloid-β 42 (Aβ42) and α-synuclein (α-Syn) can coassemble. This has motivated us to investigate the interaction between their monomers as a first step toward exploring the possibility of forming heterodimeric complexes. In particular, our study involves the utilization of various Amber and CHARMM force-fields, employing both implicit and explicit solvent models in replica exchange and conventional simulation modes. This comprehensive approach allowed us to assess the strengths and weaknesses of these solvent models and force fields in comparison to experimental and theoretical findings, ensuring the highest level of robustness. Our investigations revealed that Aβ42 and α-Syn monomers can indeed form stable heterodimers, and the resulting heterodimeric model exhibits stronger interactions compared to the Aβ42 dimer. The binding of α-Syn to Aβ42 reduces the propensity of Aβ42 to adopt fibril-prone conformations and induces significant changes in its conformational properties. Notably, in AMBER-FB15 and CHARMM36m force fields with the use of explicit solvent, the presence of Aβ42 significantly increases the β-content of α-Syn, consistent with the experiments showing that Aβ42 triggers α-Syn aggregation. Our analysis clearly shows that although the use of implicit solvent resulted in too large compactness of monomeric α-Syn, structural properties of monomeric Aβ42 and the heterodimer were preserved in explicit-solvent simulations. We anticipate that our study sheds light on the interaction between α-Syn and Aβ42 proteins, thus providing the atom-level model required to assess the initial stage of aggregation mechanisms related to Alzheimer's and Parkinson's diseases.

The graphic shows:
- **Highly stable heterodimer model**
  - Stronger interactions compared to Aβ dimer
- **Increased β-content in a heterodimer**
- **Assessment of binding interface and affinities**
  - Aβ C-terminal residues plays crucial role
- **Comparative analysis of REMD implicit and conventional explicit solvent simulations using both Amber and CHARMM**

α-synuclein + amyloid β 42 → diverse initial conformations → Replica-exchange molecular dynamics simulations → heterodimer

1. INTRODUCTION

Amyloid-β (Aβ) and α-synuclein (α-Syn) are typically soluble proteins that can form neurotoxic aggregates associated with Alzheimer's (AD) and Parkinson's disease (PD), respectively. However, an overlap of pathologies is found in the case of dementia with Lewy bodies (DLB),[1−3] which is a more general term to refer to diffuse DLB,[4] DLB,[5] cortical DLB,[6] and senile DLB.[7] Several studies suggest that Aβ and α-Syn coassemble, but the role of α-Syn in amyloid plaque formation requires further investigation.[2,8−12] Here, we explore the possibility of forming heterodimeric structures from Aβ42 and α-Syn by means of all-atom molecular dynamics (MD) simulations. Toward our goal, we analyze various properties elucidating the behavior of these molecules in the heterodimer and the respective monomeric structures. Thus, we anticipate that our results might have implications in assessing aggregation mechanisms related to AD and PD.

α-Syn is a protein composed of an N-terminal domain (residues 1−60), a variable internal hydrophobic nonamyloid component (NAC) domain (residues 61−95), and a variable C-terminal acidic tail (residues 96−140), mainly consisting of negatively charged glutamate and aspartate residues.[11,13] The middle 35-amino acid NAC domain is the building block of α-Syn aggregates.[14] The structure of α-Syn depends on its environment, being natively unfolded in an aqueous solution, an α-helical conformation when bound to lipid vesicles, or β-pleated sheets in aggregates.[11] In cells, two forms are found: an
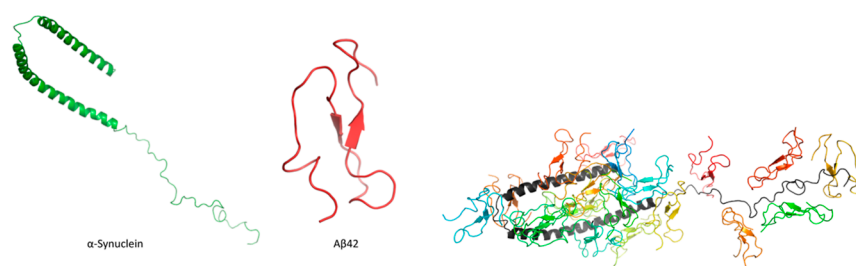
Figure 1. Cartoon representations of monomeric α-Syn (PDB id: 1XQ8), Aβ42,[47] and 20 orientations of α-Syn−Aβ42 heterodimers used as initial configurations in the REMD simulations.

α-helix-rich membrane-bound form and a disordered free cytosolic form.[15] Recent studies show that not only fibrils but also α-Syn and Aβ oligomers possess neurotoxic properties.[16−18]

Aβ has three positively and six negatively charged amino acids with its structure found in both membrane-associated and aqueous environments.[19,20] Moreover, Aβ42 has a higher propensity for aggregation than Aβ40, despite representing only about 10% of the secreted Aβ,[21] while it can act as a seed for Aβ40 aggregation in vitro.[22,23] Given the importance of Aβ42 in the formation of Aβ plaques and the fact that α-Syn interacts differently with Aβ42 than with Aβ40,[24−27] our focus in this study will only be on the interaction between Aβ42 and α-Syn. Previous in vitro and in vivo experiments have suggested a direct interaction between Aβ and α-Syn,[8,9] confirmed in both human and mice brain samples with overlapping pathologies.[10,28] Indeed, results obtained by NMR spectroscopy suggest that membrane-bound α-Syn interacts with membrane-associated Aβ42, while Aβ42 may also cleave the NAC fragment of α-Syn.[11] Moreover, Aβ42 is eventually precipitated with the NAC according to neuropathological observations in DLB patients.[29,30] In a recent experimental study by Köppen et al.,[31] the effect of a minor concentration of Aβ42 and pGlu-Aβ42(3−42) on the aggregation propensity of α-Syn has been investigated. The authors found that the interaction of α-Syn with Aβ leads to accelerated fibril formation and enhanced nucleus formation. These effects can be explained to a certain extent by monitoring the structural changes of the two molecules upon their interaction. To this end, previous experimental studies have investigated the different structural forms of α-Syn and the different effects on Aβ aggregation.[32] In particular, it has been found that fibrillar α-Syn favors the heterogeneous nucleation of Aβ aggregates, in contrast to monomeric α-Syn. The authors have attributed this effect to differences in concentration between the monomeric and the fibrillar α-Syn cases. Although these experiments have provided important insights into the Aβ and α-Syn coaggregation mechanisms, a detailed understanding of the interaction between these two molecules is still lacking. The development of structure prediction tools has drastically improved with the release of AlphaFold2,[33] however, it also has its limitations, being unable to predict dynamics, the effect of the environment on structure and dynamics, and its efficiency drops down significantly for proteins for which there are no or very few structures available with similar sequences. For example, an attempt to use the AlphaFold-Multimer[34,35] for the prediction of α-Syn−Aβ42 heterodimer results in a structure with a very low confidence score.

There are many approaches to lower the cost of computational studies and allow the study of larger systems over longer time scales, enabling the observation of large conformational changes in the studied systems rather than local fluctuations. For example, replica exchange MD[36,37] simulations involve running many trajectories simultaneously at various temperatures, allowing for efficient crossing of energy barriers in higher temperature replicas. On the other hand, the use of graphical processing units (GPUs) can speed up simulation by approximately 2 orders of magnitude compared to the use of central processing units (CPUs).[38,39] Although the use of GPUs is not limited to conventional MD simulations, its efficiency for REMD simulations is significantly lower.[40] Another approach is to use simplified models, namely, coarse-grained models, in which the number of interaction centers and degrees of freedom is severely reduced, smoothing out the energy landscape. This allows for more than a 2−3 orders-of-magnitude speed-up.[41] However, such methods can lose important details and are prone to inaccuracies, especially in the case of disordered systems. Another approach is to use an all-atom representation of the solute but use a mathematical function to describe its interaction with the solvent, called an implicit solvent model.[42] This approach is especially useful if the studied system is largely disordered and forms noncompact conformations, as such systems would require large simulation boxes if explicit solvent would be selected, even in the presence of periodic boundary conditions. However, similarly to the use of a coarse-grained approach, the simplifications used may lead to inaccuracies.[43]

Although improvements in both hardware and software have allowed for the achievement of time scales of multiple microseconds in all-atom force fields for small and medium-size systems using GPUs, this is still far from the fibril-formation time scales of hours and days. Therefore, in this work, we focused on the initial aggregation events related to monomeric Aβ42 and α-Syn, as well as their heterodimer, in implicit and explicit solvent simulations instead. Due to computational restrictions, large-scale implicit solvent REMD simulations in the Amber all-atom force field were coupled with GPU-accelerated conventional MD explicit solvent simulations in AMBER-FB15[44,45] and CHARMM36m[46] force fields. Based on a detailed atomic-scale analysis of a range of properties, we identified key conformational changes for α-Syn and Aβ42 monomers, as well as interactions that crucially contribute to different behaviors in the heteromeric structure compared to the respective monomeric structures. Moreover, we confirmed the possibility of heterodimer formation, identified its structure, and provided a comparison between implicit and explicit solvent treatments of monomeric and heterodimeric forms of both molecules, including multiple Amber and CHARMM36m force fields. Thus, we anticipate that our results will have further implications for a better understanding of the coassembly of α-Syn and Aβ42 chains.

Table 1. Types of Simulations Performed in This Study: REMD Simulations in Implicit Solvent of Aβ42 and α-Syn Monomers and Their Heterodimer; Folding Conventional MD Simulations of α-Syn in Explicit Solvent; Stability Determination of Aβ42-α-Syn Heterodimer in Explicit Solvent Conventional MD Simulations; Conventional MD Simulations to Estimate Binding Affinity of Aβ42 and α-Syn Dimers

| system	force field	solvent	trajectories	total time [μs]	temperature [K]
Aβ42	Amber ff14SBonlysc	GB-Neck2	20 × 4000 ns	80	281−512.19
α-Syn	Amber ff14SBonlysc	GB-Neck2	20 × 2000 ns	40	281−512.19
Aβ42-α-Syn	Amber ff14SBonlysc	GB-Neck2	20 × 1150 ns	23	281−512.19
α-Syn	AMBER-FB15	TIP3P-FB	3 × 1667 ns	5	300
α-Syn	CHARMM36m	TIP3P*	3 × 1667 ns	5	300
Aβ42-α-Syn	AMBER-FB15	TIP3P-FB	5 × 1000 ns	5	300
Aβ42-α-Syn	CHARMM36m	TIP3P*	5 × 1000 ns	5	300
α-Syn-α-Syn	AMBER-FB15	TIP3P-FB	3 × 5 × 50 ns	0.75	300
Aβ42-Aβ42	AMBER-FB15	TIP3P-FB	3 × 5 × 50 ns	0.75	300
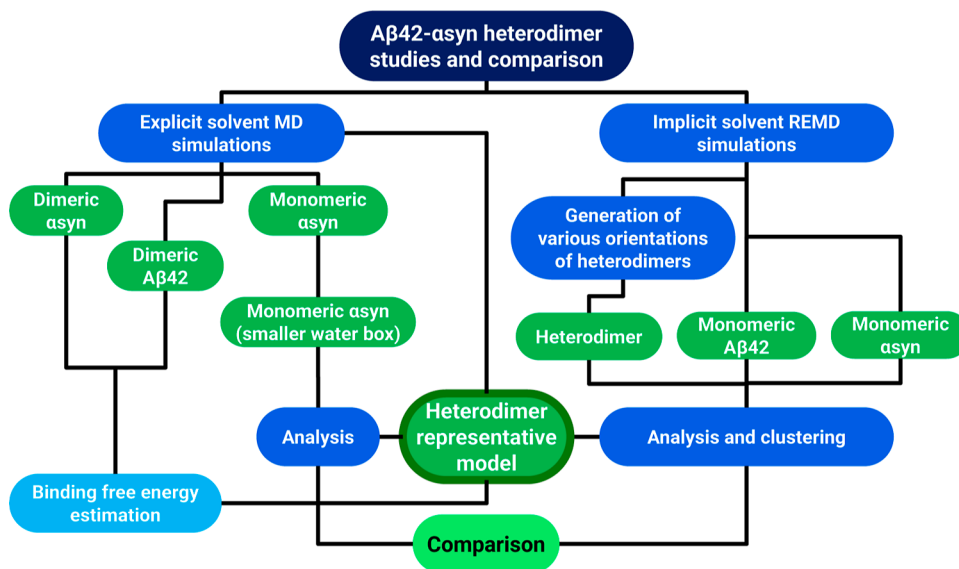
Figure 2. Schematic visualization of the flowchart presenting simulations and analyses performed in this work.

2. METHODS

2.1. Initial Structures Used in the Simulations. In this study, we employed MD to simulate three different systems: monomeric α-Syn, monomeric Aβ42, and their heterodimer (Figure 1). The initial structure of α-Syn was adapted from the Protein Data Bank (PDB id: 1XQ8), while the initial structure of Aβ42 is the one proposed by Yang and Teplow[47] (Figure 1). MD simulations of monomeric systems were utilized to evaluate and compare the performance of implicit and explicit solvent approaches, both with each other and with experimental data. Additionally, they were used to estimate conformational changes upon heterodimer formation.

We generated 20 initial conformations of the heterodimer using the preparatory step of the UNRES-Dock algorithm.[48] This step places chains of the molecules in as different orientations as possible, with the condition that the chains have to form at least one interaction. Using such an approach, instead of complete docking, allowed us to avoid any bias arising from the initial structures being stuck in the local minimum of the energy and speed up the equilibration process. Moreover, it was not expected for the monomeric forms of Aβ42 and α-Syn to remain in the initial conformations during REMD simulations due to their intrinsically disordered character and the fact that the monomeric α-Syn conformation was obtained experimen-

tally in a micelle, and it substantially varies from the aqueous environment.

The types of MD simulations performed in this study are summarized in Table 1, while additional information can be found in Table S1. The workflow of the simulations is shown in Figure 2. Initial and final conformations from each simulation are attached to the Supporting Information.

2.2. Implicit Solvent Simulations of Monomers and the Heterodimer. To extensively search the conformational space of monomeric and heterodimeric forms of α-Syn and Aβ42, the replica exchange molecular dynamics (REMD)[36,37] sampling method was selected, as it allows crossing energetic barriers at higher temperatures. However, this approach requires the use of many trajectories (replicas) to ensure proper performance and cannot be efficiently performed with GPU acceleration. Moreover, due to the intrinsically disordered character of both α-Syn and Aβ42, there is an abundance of extended molecular conformations. Hence, a large simulation box is required, especially in the case of α-Syn (with a maximum distance between atoms in PDB 1XQ8 close to 160 Å), to avoid the interaction between periodic images of the molecule.

This translates to large requirements for excessive computation time when explicit solvent conditions are considered, and GPU-accelerated simulations are unavailable for extensive REMD sampling. Therefore, we used an implicit solvent

model to conduct our simulations, resulting in a significant speed-up compared to the corresponding explicit solvent model, which should not compromise the accuracy of the simulations.[45,49] In particular, the implicit generalized Born scheme was used to simulate our systems, as implemented in the AMBER20 package,[50] using the ff14SBonlysc force-field with mbondi3 radii.[49] Several studies suggest that the combination of ff14SBonlysc with the GB-Neck2 model provides reasonable results regarding the prediction of protein folding mechanisms.[45,49] Moreover, the standard version of AMBER ff14SB was found to provide good agreement with available experimental data for Aβ.[51,52]

To deal with the rough energy landscape that stems from the use of all-atom force-fields and enhance the sampling of the conformational space, we carried out REMD simulations with 20 replicas with temperatures ranging from 281 to about 512 K (Table S2). The temperature was controlled through a Langevin thermostat for each replica, and the equations of motion were integrated with a leapfrog algorithm as implemented in the AMBER20 package.[50] The temperature distribution of the replicas was generated by a temperature generator[53] to provide satisfactory exchange rates.

To prepare monomeric and heterodimeric systems for the REMD simulations, their energy was minimized using 7000 steps of the steepest descent and 3000 steps of the conjugate gradient method. Then, the systems were gradually heated up and relaxed at each individual temperature for 5 ns by employing conventional simulation in the canonical ensemble with the Langevin thermostat. Simulations using the implicit solvent model were performed with an infinite cutoff for long-range interactions. During the REMD simulations, exchanges between the different replicas were attempted every 500 steps, where the time step in the simulations was set to 2 fs.

Trajectories for monomeric systems reached a length of 4 μs for Aβ42 and 2 μs for α-Syn per replica, translating into 80 and 40 μs of total simulation time, respectively, while the heterodimeric system was simulated for 1 μs (20 μs of total simulation time) due to its larger size.

To ensure proper sampling in the case of the heteromeric system, each replica started from a different initial orientation of the chains (Figure 1), as mentioned in the above section. The analysis of our results is based on the trajectories obtained from the REMD simulations for both the monomeric and the heteromeric systems at temperature T = 300.69 K. It should be noted that this temperature is lower than the physiological temperature of approximately 310 K. However, it is a typical temperature at which protein force fields are usually optimized and tested and at which most simulations are performed. Therefore, it was selected to ensure high reliability and consistency with existing data, however, it is expected that there should not be any substantial changes between trajectories at 300 and 310 K.

2.3. Explicit Solvent Simulations of Monomers and the Heterodimer. To compare the behavior of the studied systems between implicit and explicit solvent models and to ensure the highest level of robustness, an additional series of explicit solvent simulations for monomeric α-Syn and the heterodimer were run in two completely different force fields. As we had previously simulated monomeric Aβ42 using multiple force fields and two sampling methods (REMD and conventional MD) in a multiple-microsecond time scale,[51] we decided to use this data for comparison. Similar to implicit solvent simulations, a Langevin thermostat was used to maintain a temperature of

300 K, while a cutoff of 9 Å was applied for long-range interactions with the PME method.[54] The selection of the AMBER-FB15 force field was dedicated to its ability to better represent conformational fluctuations of the studied systems away from equilibrium, while coupling with the TIP3P-FB water model provides higher and closer-to-experiment values of the radius of gyration,[55] which is expected for disordered systems. CHARMM36m is a modification of the CHARMM36 force field,[56] which should provide satisfactory accuracy for both folded and intrinsically disordered peptides and proteins[46] and has been found to be among the top force fields to study various IDPs.[57] Parameters for the AMBER-FB15 force field were generated using tLeap, part of the AmberTools package, while CHARMM36m parameters were generated by the use of the CHARMM-GUI server.[58] In explicit solvent simulations, all protein systems were surrounded by a layer of water using the recommended water model, while Na⁺ and Cl⁻ ions were added to neutralize the charge and reach a physiological concentration of approximately 150 mM.

2.3.1. Folding of the Monomeric α-Syn. The experimental monomeric α-Syn structure (PDB: 1XQ8) is in an extended conformation, as it was bound to a micelle in the NMR experiment, therefore, it is expected that its conformation in solution would be significantly different. Therefore, we first ran a short 100 ns run in a very large explicit solvent box (165 × 165 × 165 Å) with approximately 112,000 water molecules to allow the molecule to reach a more compact structure. Then, a second series of MD simulations (each consisting of three 1.67 μs trajectories, resulting in a total time of 5 μs per system) was run, as previously mentioned, but in a significantly smaller periodic box (91 × 91 × 91 Å) with approximately 19,000 water molecules both in AMBER-FB15 and CHARMM36m force fields.

2.3.2. Studies of α-Syn−Aβ42 Heterodimer Stability. A series of five trajectories, each of 1 μs length, resulting in a total time of 5 μs per system, starting from the most probable conformation of the α-Syn−Aβ42 heterodimer, was performed with the AMBER-FB15 force field[55] and the TIP3P-FB water model,[59] and the CHARMM36m force field with the modified TIP3P model. The use of a different force field compared to the implicit solvent simulations was motivated by the need to verify the stability of the heterodimer regardless of the simulation details.

The system was neutralized and placed in a periodic boundary box together with approximately 20,000 water molecules, providing a layer of about 18 Å around the protein complex. Due to the use of the equilibrated structure for the heterodimer, a reasonable size of the periodic box could be employed, in contrast to the implicit solvent simulations where extended disordered conformations were used as initial configurations for the simulations. The system's energy was minimized, followed by equilibration (1 ns), and then production runs, consisting of five trajectories, each of 1 μs, were performed in explicit solvent.

2.3.3. α-Syn−Aβ42 Heterodimer and Aβ42 Dimer Binding Energies. To compare the binding free energies, five short MD simulations (each of 50 ns) were conducted for three Aβ42 models and three α-Syn dimeric models, as predicted in previous studies.[60,61] The simulations used the same conditions as the explicit water simulations described above, employing the AMBER-FB15 force field[55] and the TIP3P-FB water model.[59] The last 10 ns of the simulations were used to perform the MM-PBSA analysis, providing an estimate of the binding free energy
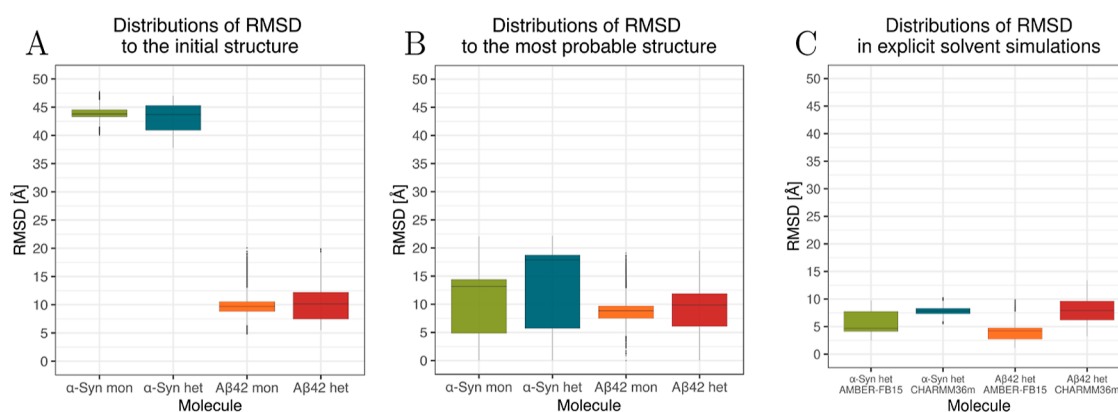
Figure 3. rmsd distributions of α-Syn and Aβ42 as monomers (mon) and in the heterodimer (het), as indicated. (A) initial, and (B) the most probable minimum free energy structure used as a reference for rmsd calculations.

for each system. Predicted values were subsequently averaged over five trajectories for each system.

2.4. Analysis. *2.4.1. Root Mean Square Deviation.* The first property we have considered in our study is the root mean square deviation (rmsd) of the atomic positions of the molecules, which is a first step toward validating the stability of our simulations. The rmsd is defined as follows

$$\text{rmsd} = \sqrt{\frac{1}{N} \sum_{i=1}^{N} \delta_i^2} \qquad (1)$$

where δ_i^2 is the distance between atom i and its position at the reference structure, which contains N atoms. As usual, only the heavy atoms (e.g., N, C, O, etc.) are considered in the rmsd calculation and the usual alignment procedure takes place before applying the above equation.

2.4.2. Radius of Gyration. As a next step in our analysis, we have monitored the radius of gyration (R_g) and the maximum radius of gyration ($R_{g\ max}$) for each chain in both the monomeric and the heteromeric cases. R_g is described by the following relation

$$R_g = \sqrt{\frac{1}{N} \sum_{i=1}^{N} (r_i - r_{com})^2} \qquad (2)$$

where r_{com} is the center of mass of the chain. N is the number of heavy atoms in each chain. $R_{g\ max}$ is the distance of the most distant atom from the center of mass.

2.4.3. Other Analysis. For analyzing properties other than rmsd and R_g, we utilized the second halves of the simulation trajectories, considering them as equilibrated portions. Secondary structure elements were determined using the DSSP algorithm[62] as implemented in the CPPTRAJ tool.[50] Solvent-accessible surface area (SASA) concerning individual residues and the whole molecules was calculated using the Linear Combinations of terms composed from Pairwise Overlaps (LCPO) method.[63] Additionally, we calculated contact maps for both monomeric and heteromeric cases. A contact was considered when at least two heavy atoms from different amino acid residues were within a distance of 0.5 nm, under the condition that in a single snapshot, only one contact could be formed within a single pair of residues. We employed a hierarchical agglomerative average-linkage clustering method to divide the ensemble of structures into five groups, and then the cluster centroid of the largest cluster was treated as the most representative structure. Free energy maps were calculated as

described in our previous work (eq 6 and its description in ref 64).

2.4.4. Binding Free Energy Analysis. Binding free energies were estimated using two approaches. In the first one, a subset of snapshots from MD trajectories was analyzed by means of the MM-PBSA method as implemented in AMBER software.[50] Due to performance limitations, 100 snapshots were used to calculate enthalpic contributions, while 10 snapshots were used to estimate entropic contributions using the normal-mode analysis method, which is a standard procedure to predict binding affinities from MD trajectories.[65] In the second approach, single representative models were used instead of ensembles of structures to predict global and per-residue binding free energies using the HawkDock server,[66] which we found to provide reasonable relative values.[67]

2.4.5. Molecular Mechanics—Poisson–Boltzmann Surface Area Method. By using the MM-PBSA method, the binding affinity (binding free energy) (ΔG_{bind}) between two molecules is composed of the following five terms

$$\Delta G_{bind} = \Delta E_{ele} + \Delta E_{vdW} + \Delta G_{sur} + \Delta G_{PB} - T\Delta S \qquad (3)$$

where ΔE_{ele} and ΔE_{vdW} are, correspondingly, electrostatic and van der Waals interaction energy; ΔG_{sur} and ΔG_{PB} are nonpolar and polar solvation energies; and $T\Delta S$ is the entropic contribution.

MMPBSA.py, a part of AmberTools, was used to calculate the binding free energy. Charges and atomic radii from the force field used for the simulation were used for calculating electrostatic and van der Waals interactions. The polar solvation energy was calculated by solving the Poisson–Boltzmann equation using the PBSA program, also a part of AmberTools, at an ionic concentration of 0.15 M. The internal and external dielectric constants were set to 1.0 and 80.0, respectively. The nonpolar solvation energy is proportional to the SASA as follows

$$\Delta G_{sur} = \alpha \cdot \text{SASA} + \beta \qquad (4)$$

where α and β were set to 0.005 and 0.0, respectively. SASA was calculated by the LCPO method[63] with a solvent probing radius of 1.4 Å. A normal mode approximation calculation was used to obtain the entropic contribution term at a temperature of $T = 300$ K.

3. RESULTS AND DISCUSSION

3.1. Implicit Solvent Simulations of Monomeric α-Syn and Aβ42 and Their Heterodimer. The first step of the
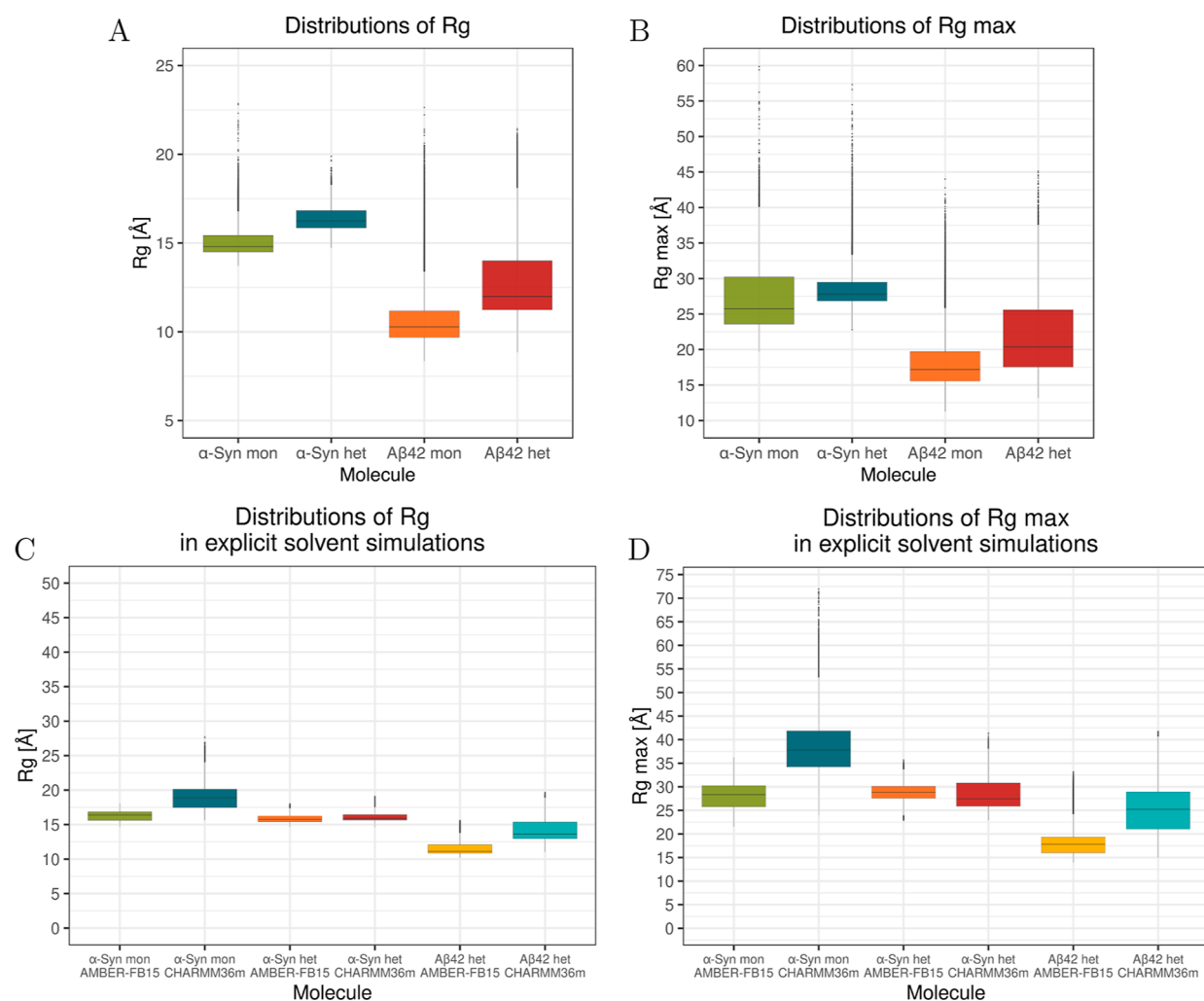
Figure 4. R_g (A) and $R_{g\,max}$ (B) distributions of α-Syn and Aβ42 as monomers (mon) and in the heterodimer (het) as indicated.

analysis involved checking whether the REMD simulations were properly configured to ensure satisfactory exchange rates and temperature walks. It is known that problems with achieving a proper exchange rate, without obtaining a good walk between various temperature replicas, in which only local exchanges between 2 and 3 neighboring replicas are observed, could effectively decrease the sampling efficiency of the REMD simulation. This effect usually worsens with an increase in system size, including both solute and solvent, and in explicit solvent simulations, it can even be observed for small systems such as monomeric Aβ42.[51] However, analysis of the implicit solvent trajectories generated in this study clearly shows that most of the trajectories successfully traverse wide ranges of temperatures (Figure S1). Even those limited to narrower temperature ranges travel between at least 7 different temperature replicas (e.g., in the temperature range of approximately 281–343 K), allowing for proper conformational search of the system. This indicates that the REMD simulations were well-configured and should provide efficient sampling of the conformational space for the studied systems.

3.1.1. Analysis of Structure Stability and Shape. We analyzed the time evolution of the rmsd (Figure S2) from the initial structures (Figure 1), revealing high stability of all systems throughout the simulations. Notably, α-Syn, in both monomeric and heterodimeric configurations, exhibited an initial hydrophobic collapse (Figure 1). This observation aligns with

expectations, given that the initial experimental structure was derived after binding to the micelle and simulations were conducted in a solution environment.

In particular, the rmsd values of α-Syn are approximately four times higher than those of Aβ42, a result of an extended initial structure and a larger chain length (Figure 3). The equilibrium rmsd values for both systems are generally high due to the disordered character of the molecules. By comparing the differences between the monomeric α-Syn and Aβ42 systems with the heteromeric one, we observe that the average values are similar. However, both α-Syn and Aβ42 molecules show larger standard deviations in the rmsd values in the heteromeric system than in the respective monomeric systems. Additionally, this difference is more pronounced in the case of Aβ42. This may be attributed to the interaction between α-Syn and Aβ42 in different orientations for various replicas, leading to average values with a larger variance. However, this observation is expected for systems that are highly disordered, especially in monomeric forms.

Our findings reveal that both α-Syn and Aβ42 exhibit larger dimensions in heteromeric systems compared to their respective monomeric counterparts (Figure 4). Although the increase in R_g is subtle, it is more noticeable for Aβ42. However, this trend is not as pronounced when examining $R_{g\,max}$, as the most distant residues from the center of mass occupy comparable positions in monomeric and heteromeric systems, despite the more compact
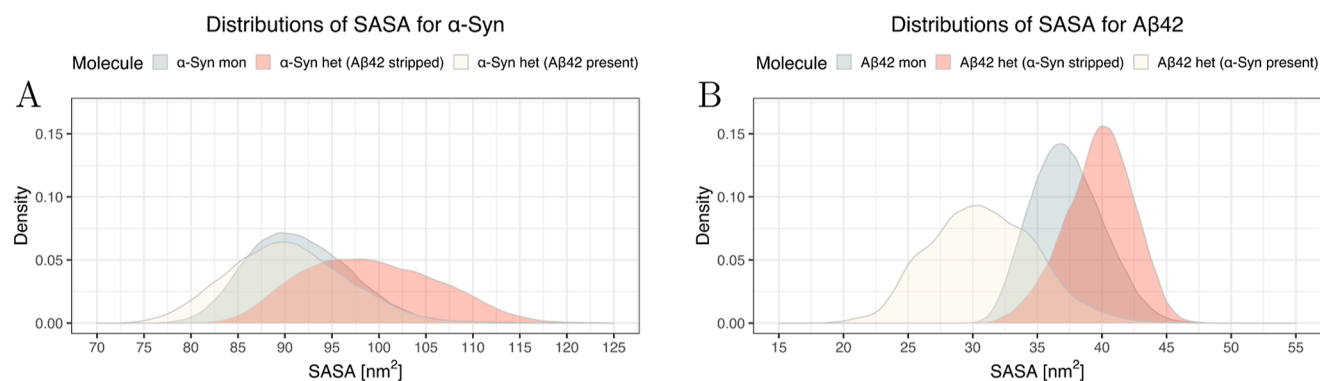
Figure 5. Distributions of SASA for (A) α-Syn and (B) Aβ42 in monomer (mon) and heterodimer (het) simulations, as indicated.

conformation of α-Syn. Generally, R_g values around 15 Å for α-Syn suggest a predominantly compact conformation during REMD simulations.[68,69] Our results imply that α-Syn may become more stable upon binding to Aβ42. Additionally, the larger standard deviation in R_g and $R_{g\,max}$ between monomeric and heterodimeric forms is more pronounced for Aβ42. In summary, the analysis of rmsd, R_g, and $R_{g\,max}$ collectively suggests that the Aβ42 chain is more influenced by the presence of α-Syn than vice versa.

Experimental R_g of Aβ42 is approximately 10.1−10.6 Å,[70,71] which closely aligns with the average R_g observed in our implicit solvent simulations of monomeric Aβ42. These results are also similar to the values observed in explicit solvent simulations.[51] On the contrary, the NMR-calculated hydration radius of α-Syn is about 29 Å. Considering the nonspherical shape of monomeric α-Syn, this would indicate an R_g above 23 Å, while the analysis of data from SAXS suggests an even larger value of 35.5 Å.[72] These values are considerably larger than the R_g range observed in our implicit solvent simulations, which focuses on the range of 14−16 Å. Analysis of the explicit solvent simulations provided an average R_g of 16.20 Å (SD: 0.54 Å) and 18.55 Å (SD: 0.42 Å) for simulations with AMBER-FB15 and CHARMM36m force fields, respectively. Although the values in CHARMM36m were higher (18.55 Å, SD: 0.42 Å), they are still significantly lower than those observed in the experiments.[72] However, it should be noted that experimental conditions may affect the monomeric α-Syn conformation, and it is challenging to ensure that α-Syn did not start to aggregate, leading to potential differences in these values. The average observed values in our simulations and other studies[72] are notably lower than those experimental values.

3.1.2. Free Energy Maps and Minimum Energy Structures. We have calculated the free energy maps as a function of R_g and rmsd for α-Syn and Aβ42 in the monomeric and the heteromeric cases (Figure S3). For both chains, the free energy maps for the heterodimer exhibit similar behavior, with multiple energy minima being distinct from each other in comparison with the more homogeneous free energy maps in the case of monomeric structures, where mostly a single minimum can be easily identified. In the case where the number of contacts is chosen as an order parameter instead of the rmsd, a single free energy minimum is mostly observed for all cases (Figure S4). By using cluster analysis, we have identified the most probable structure for α-Syn and Aβ42, and we have recalculated the rmsd with respect to these structures. Clearly, the rmsd is significantly smaller in the case of α-Syn (about 14 Å) and also smaller in the case of Aβ42 (about 9 Å, Figure 3). Both α-Syn and Aβ42 chains

exhibit larger rmsd in the heteromeric case, where the standard deviation is smaller in the case of α-Syn than in the case of Aβ42. This shows that the α-Syn molecule exerts a greater influence on Aβ42 than Aβ42 on α-Syn.

3.1.3. Fluctuations of Structure Elements during Simulations. By using average conformations from the respective trajectories as reference structures for α-Syn and Aβ42, we calculated the root-mean-square fluctuations (RMSF) for each residue (Figure S5). Interestingly, the differences between the monomeric and heteromeric cases are small for Aβ42. In contrast, the α-Syn atoms in the heterodimer case exhibit larger fluctuations from their average positions compared to those in the α-Syn monomeric case. In particular, significant differences occur along the entire α-Syn chain, especially in residues 26−63, 98−107, and 116−123. Experimental studies by Gallardo et al. show that although the N-terminus of α-Syn has some helical propensity, the C-terminus is disordered due to its acidic character,[73] which is consistent with the high structural fluctuation of the C-terminus in the heterodimer observed in our study. Although rmsd suggests otherwise, the local fluctuations of α-Syn atoms (RMSF) show larger deviations from their reference positions than those seen in the case of Aβ42. However, it should be noted that RMSF analysis is performed with respect to the average conformations, which can significantly vary and provide only a rough estimation due to the disordered character of the studied molecules, especially in the case of a heterodimer, in which in addition to the conformations close to the most probable orientation of the molecules, a small number of snapshots with less probable orientations can be present due to the nature of REMD simulations, increasing the base value of the RMSF. Most of the less flexible fragments of α-Syn are located in the regions interacting with Aβ42, e.g., residues 24−26, 69−71, and 109−115.

3.1.4. α-Syn−Aβ42 Heterodimer Allows for the Formation of the Hydrophobic Core between the Molecules. The comparison of SASA values in monomeric and heterodimeric forms (Figure 5) shows that there is no significant difference for α-Syn. This can be attributed to the size discrepancy between the molecules and the presence of a large unbound part of α-Syn to Aβ42, which compensates for the SASA difference. The presence of α-Syn is causing a drastic change to the Aβ42 SASA, which decreases by 7 nm^2, namely, from 37 to 30 nm^2. This significant difference suggests a higher hydrophobicity of Aβ42 compared to α-Syn. In general, SASA values for monomeric Aβ42 are in agreement with previous observations, where high flexibility of the chains was obtained,[74,75] e.g., by using REMD sampling.[51]

Table 2. Average Secondary Structure Content Obtained in This Study for Monomeric Aβ42, α-Syn in Implicit and Explicit Solvent and Their Heterodimer and Literature Ranges for Monomeric Aβ42[a]

molecule	FF_{solvent}	β-sheets (%)	α-helix (%)	turn (%)	coil (%)
Aβ42_{mon}	ff14SBonlysc_{GB−Neck2}	27.92 (7.18)	9.97 (4.64)	20.68 (3.24)	41.43 (4.57)
Aβ42_{mon}[51]	CHARMM36m_{TIP3P*}	23.8 (14.6)	2.1 (3.9)	12.1 (5.6)	62.0 (15.8)
Aβ42_{het}	ff14SBonlysc_{GB−Neck2}	34.57 (4.70)	5.93 (4.27)	15.81 (4.08)	43.69 (3.88)
Aβ42_{het}	AMBER-FB15_{TIP3P−FB}	30.77 (3.83)	9.79 (4.84)	18.41 (4.92)	41.03 (7.06)
Aβ42_{het}	CHARMM36m_{TIP3P*}	24.01 (4.16)	4.18 (1.82)	13.07 (4.30)	58.73 (4.03)
α-Syn_{mon}	ff14SBonlysc_{GB−Neck2}	19.60 (6.86)	22.40 (6.22)	18.18 (1.59)	39.82 (2.56)
α-Syn_{mon}	AMBER-FB15_{TIP3P−FB}	1.06 (0.56)	43.59 (1.50)	17.70 (2.33)	37.66 (1.35)
α-Syn_{mon}	CHARMM36m_{TIP3P*}	3.36 (1.34)	31.04 (7.98)	6.09 (0.97)	59.50 (6.19)
α-Syn_{het}	ff14SBonlysc_{GB−Neck2}	21.05 (4.74)	15.99 (5.11)	17.84 (1.34)	45.12 (4.83)
α-Syn_{het}	AMBER-FB15_{TIP3P−FB}	24.69 (2.40)	18.22 (1.74)	15.16 (2.17)	41.93 (1.86)
α-Syn_{het}	CHARMM36m_{TIP3P*}	18.76 (2.68)	17.12 (4.00)	12.68 (2.28)	51.45 (4.94)

[a]Indexes: mon—monomeric form, het—in heterodimer. Value for monomeric form of Aβ42_{mon} in CHARMM36m is taken from previous study.[51] Values in brackets, if present, show standard deviations.

There are substantial differences in SASA values for Aβ42 upon binding to α-Syn: the average SASA decreases by about 20%, however, when considering the theoretical SASA of Aβ42 in the heterodimer with α-Syn removed from analysis, the average SASA increases by about 11%. This suggests that interactions between complexes predominantly involve hydrophobic residues, forming a hydrophobic core upon complex formation to shield these residues from water molecules. The SASA difference per residue (Figure S6) affirms that binding is more favorable for Aβ42 than for α-Syn, as the former can effectively reduce unfavorable interactions with water. Notably, the difference in per residue SASA upon binding is most pronounced (above 0.4 nm²) for specific Aβ42 residues: Leu17, Phe19, Phe20, Ile31, and Ile32.

The total size of the binding interface of the α-Syn−Aβ42 heterodimer is equal to 10 nm² for each of the molecules (this translates to approximately 11 and 33% of Aβ42 and α-Syn, respectively, being involved in the interactions within the heterodimer), indicating a significant reduction in hydrophobicity within the binding region. This also elucidates why the impact of α-Syn on Aβ42 is much larger than the impact of Aβ42 on α-Syn, as a larger portion of Aβ42 is involved in interactions with its partner in the heterodimer. It should be noted that the varying degrees of the effects of one system on the other are also caused by the size difference between the molecules, with α-Syn having 233% more amino acid residues than Aβ42. As the hydrophobic interactions between α-Syn and Aβ42 are important for the formation of the heterodimer and the presence of α-Syn causes a drastic change to the Aβ42 SASA, it indicates a higher hydrophobicity of Aβ42 compared to α-Syn. This, together with significant size difference, likely makes Aβ42 more susceptible to the influence of α-Syn binding compared to the reverse situation.

3.1.5. Secondary Structure Content. In the absence of α-Syn, the β-content of Aβ42 (27.92%) (Table 1) is consistent with the result (26.2%) obtained by using the OPLS/AA force field and GB implicit solvent,[76] but much higher than the 10% predicted by the AMBER force field ff99SB and water model TIP3P.[60] Overall, our result falls into the experimental[26,77] and theoretical[51,78−81] range of 9−27%. Similar to previous works (see Review[82]), the helix structure (9.97%) (Table 1) is less populated than the β strand, and the coil is more abundant than the turn. Experimental circular dichroism (CD) spectroscopy studies estimate the α-helical content between 3 and 9% for monomeric Aβ42.[26,77] In our simulations, the helix structure is

slightly more pronounced, which is partially caused by the use of implicit solvent. Nevertheless, this value is in the range found in other MD studies.[51]

The analysis of secondary structure for both the α-Syn and the Aβ42 (Table 2) indicates that in the case of the heterodimer, the β-sheet content slightly increases, whereas the α-helix content decreases. The turns remain the same for Aβ42, while a decrease is observed in the case of α-Syn. Finally, the coil increases for both α-Syn and Aβ42 in the heterodimer case. All these changes are not statistically important due to the large standard deviations of secondary structure contents. Experimental studies suggest that monomeric α-Syn possesses a high α-content upon contact with lipids, which shifts to an abundance of β-structures in water.[83] In our studies, α-Syn is present in the intermediate state, in which both α- and β-contents are high due to the disordered character of the molecule. In general, our results are in agreement with experimental and discrete MD (DMD) studies, which showed that α-Syn can form both α-helices (mostly residues 8−32) and β-sheets (mostly residues 35−56 and 61−95), while the C-terminus remains unstructured.[73,84]

Analysis of the secondary structure of the given amino acid residues (Figure S7) shows that there are no significant changes in the tendency of given residues to form a particular type of secondary structure. For α-Syn, we did not observe large similarities to secondary structure propensities to form mostly α-helices for residues 1−60, β-sheets for 61−95, and an unstructured part for 96−140, which is established experimentally.[85] This indicates that the monomeric structure is much different than fibrillar. Residues 45−57 and 71−82 are known to be responsible for α-Syn aggregation and its pathogenic properties.[83,86] Our studies show that the β-structure of the latter part is disturbed upon the binding of Aβ42 (Figure S7), especially residues 72 and 74, which stopped forming β-sheets. Also, the region before and including NAC (or even residues 9−89 if connected to the membrane[87]) is responsible for forming α-helices in monomeric and tetrameric forms of α-Syn,[88] which is disturbed upon Aβ42 binding.

While the secondary content of monomeric Aβ42 in implicit solvent simulations is similar to that in explicit solvent simulations performed in previous studies,[51] indicating only a small overstabilization of secondary structure elements, the secondary content of monomeric α-Syn in implicit solvent simulations is significantly different from that in explicit solvent simulations. This is especially visible in the significantly larger contribution of β-structures (19.60% compared to 1.06 and
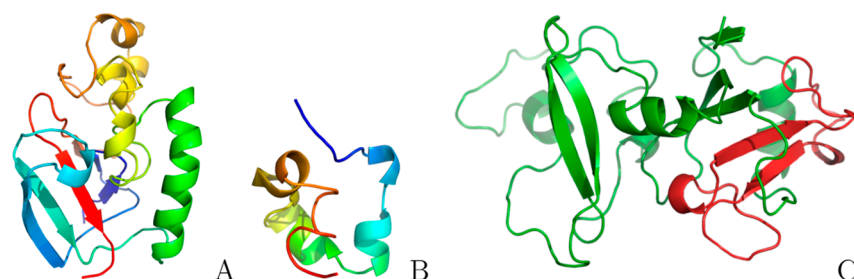
Figure 6. Representative structures of (A) α-Syn, (B) Aβ42, and (C) heterodimer determined from clustering of the free energy minimum basins of implicit solvent simulations, presented in cartoon representation.

3.36%). Similarly, as for the heterodimer, CHARMM36m determines larger unstructured fragments of monomeric α-Syn than implicit and explicit solvent simulations in Amber force fields.

It should be noted that these results are very difficult to compare to experimental data because experimental studies cannot truly observe monomeric conformations due to the relatively high concentration of studied compounds necessary in such experiments, which causes rapid α-Syn aggregation.[89] The formation of β-hairpin by residues 38−53 (by two regions rich in β-structures: 38−44 and 47−53) was found to be crucial for α-Syn aggregation in computational studies using a hybrid-resolution model.[90] Our studies show that the first of these fragments often formed β-structures in both monomeric and heterodimeric forms, and it is involved in the interaction interface with Aβ42, suggesting similarities between binding modes of fibrils and the α-Syn−Aβ42 heterodimer.

3.1.6. Similarities to Fibril Structures. Using lattice models, Li et al.[91] showed that the fibril formation time exponentially increases with the population of the so-called fibril-prone conformation **N*** in the monomeric state. **N*** is defined as the monomer conformation in the fibril state. The relationship between the aggregation rate and the population of fibril-prone conformation has been confirmed by off-lattice coarse-grained[92] and all-atom[93] simulations. Therefore, it is interesting to know how the presence of a foreign chain affects the population of **N*** of a given chain.

We have not often detected fibril-like Aβ42 structures during the simulations. Some fibril-like conformations were mostly obtained in the first half of the simulations (not equilibrated ones), which indicates that chains are generally flexible during the simulations, but such a conformation is not energetically preferable. Although generally rare, Aβ42 more often obtained S-shape conformation rather than U-shape; however, the similarity varied depending on the (proto)fibrillar structures used as a reference within a given class. In addition, the probability of fibril-like structures decreases further in the presence of α-Syn (Tables S3 and S4). Thus, we anticipate that Aβ fibril formation slows down in the presence of α-Syn. Similar behavior, but to a lesser extent, was observed for α-Syn, which did not often form fibril-like conformations, and the Aβ42 binding decreased this probability even further (Table S5). To calculate the population of **N*** conformation, we took into account only residues 17−40 and 61−95 for Aβ42 and α-Syn, respectively, which are ordered in the fibril state.

3.1.7. Intramolecular and Intermolecular Contacts. We have followed the time evolution of intramolecular and intermolecular contacts for both α-Syn and Aβ42 in both monomeric and heterodimeric forms (Figure S8) to observe that the fluctuation in the number of contacts is suppressed in the

case of the heteromeric structure, while the average number of contacts remains similar. Our conclusions are valid for both α-Syn and Aβ42 cases. In particular, the number of intermolecular contacts in the heterodimer exhibits larger variation during the course of the simulation (Figure S7) than for intramolecular contacts. We observe that α-Syn and Aβ42 establish about 10−15 contacts on average. We can identify the most important contacts by determining the contact map of the intermolecular contacts (Figure S8). First of all, we find that contacts are well spread between different parts of the chains, suggesting that our simulation protocol offers adequate sampling across the spectrum of states. Additionally, many of the contacts have as high as 18% probability of occurring during the simulation.

We have identified the most frequent residue contacts, which are listed in Table S6. From the point of view of α-Syn, intermolecular contacts usually occur in the N-terminal domain, and even more contacts appear between the negatively charged C-terminal domain of α-Syn and Aβ42. Most contacts are established between the charged parts of the two different chains. From the point of view of Aβ42, contacts between residues 16−18 and 29−35 of Aβ42 and α-Syn appear frequently. This behavior is also reflected in the case of intramolecular contact maps when comparing the monomeric and heteromeric cases for individual chains (Figure S8). Finally, we have identified the heterodimeric structure with the highest probability based on detailed contact map and free energy map analysis, presented in Figure 6.

α-Syn forms strong interactions with Aβ42 by residues 26−28, 36−37, and 69−71 with frequencies of about 25% based on REMD simulations at approximately 300 K. These fragments align well with previous observations based on MD studies that imperfect repeats R3 (residues 31−41) and R6 (residues 68−78) play a crucial role in α-Syn aggregation and may be used as potential targets for inhibitors.[94]

3.2. Explicit Water Simulations of the α-Syn−Aβ42 Heterodimer. In our investigation, three out of five trajectories, as obtained with AMBER-FB15, exhibited rmsd values under 6 Å, while the other two trajectories remained just under 10 Å (Figure S9). Notably, these fluctuations predominantly originated from flexible regions in both molecules, with α-Syn, being a larger molecule, contributing more significantly. In contrast, explicit solvent simulations in CHARMM36m displayed slightly larger structural fluctuations, characterized by an average rmsd of approximately 8 Å after 700 ns, with all trajectories exhibiting similar behavior. This differed from AMBER-FB15 simulations, where two out of five trajectories presented significantly larger rmsd values than the remaining three. Both rmsd and R_g plots (Figures S9−S10) indicate stabilization of the system after 700 ns in both force fields. Therefore, our analysis focused on the range from 700 to 1000

ns, assuming convergence. This approach also helped mitigate bias arising from utilizing the representative model from implicit solvent simulations as the initial structure for explicit solvent simulations.

Analyzing fluctuations in amino acid residues from AMBER-FB15 simulations revealed that the structure of Aβ42 was considerably more stable than that of α-Syn, with only residues 22−27 displaying larger fluctuations. In α-Syn, multiple regions, particularly in the C-terminal part not involved in binding with Aβ42, exhibited significant fluctuations. This contrasts results obtained from implicit solvent REMD simulations, where fluctuations in the heterodimer, especially in α-Syn, were larger than in monomeric structures. This discrepancy is reasonable due to the presence of multiple binding modes in the complex, causing variations in different parts of the molecules. Intriguingly, RMSF plots for CHARMM36m closely resembled those for AMBER-FB15, indicating similar regions of high flexibility in the heterodimer. Explicit solvent MD simulations for both force fields slightly decreased the compactness of the heterodimer, more pronounced in CHARMM36m, where an increase in R_g by about 1−2 Å was observed. This behavior aligns with the generally lower compactness of conformations observed in this force field.[46]

The most notable distinction between implicit and explicit solvent simulations emerged in monomeric α-Syn. Implicit solvent simulations significantly overpredicted the β-content, whereas explicit solvent simulations for the heterodimer in both solvents showed no significant changes in secondary structure distribution. While AMBER-FB15 exhibited a slight tendency to increase the content of α-helices and β-sheets, resulting in a small decrease in unstructured fragments compared to implicit solvent simulations, CHARMM36m displayed the opposite behavior, slightly increasing the percentage of unstructured fragments of the heterodimer by a small reduction in β-sheets and turns (Table 2). Despite some conformational fluctuations observed in explicit solvent simulations, they did not significantly impact the secondary structure content of the heterodimer, which remained stable during explicit solvent simulations, maintaining an average similar to implicit solvent simulations (Figure S7).

In summary, both force fields, employing the explicit solvent model, demonstrated slightly larger flexibility and less compactness of the heterodimer. However, the complex remained stable in all trajectories, confirming the high stability of the predicted model.

3.2.1. Aβ42 Increases α-Syn Aggregation Propensity. It has been demonstrated that the β-content of the monomer determines the propensity for aggregation: the higher the β-content in the monomeric state, the faster aggregation occurs.[95] To investigate whether the presence of Aβ42 accelerates α-Syn aggregation, we compare the β-contents of α-Syn in the absence and presence of Aβ42. In implicit water simulations with ff14SBonlysc$_{GB-Neck2}$, the β-content of α-Syn monomer (19.60 ± 6.86) is similar to that in the heterodimer (21.05 ± 4.74) (Table 2). However, the situation changes significantly in explicit water simulations. The presence of Aβ42 increases the β-content from 1.06 ± 0.56 to 24.69 ± 2.40 (AMBER-FB15$_{TIP3P-FB}$) and from 3.36 ± 1.34 to 18.76 ± 2.68 (CHARMM36m$_{TIP3P*}$). The impact of Aβ42 on α-Syn aggregation is not observed in implicit water models, further showing a significant overestimation of the stability of monomeric α-Syn. However, the β-content of the α-Syn-Aβ42 in the implicit solvent simulations falls between the observed

values for explicit solvent simulations in AMBER15-FB and CHARMM36m. On the other hand, explicit water models capture the experimental observation of enhanced α-Syn aggregation by Aβ42.

3.2.2. Prediction of Amino Acid Residues Involved in Binding Interface. The contact map reveals that there are several interactions between residues, which are responsible for the binding (Figure S11). Phe19, Phe20, Ile31, Ile32, Gly37, and Gly38 from Aβ42 are forming stable contacts with Val26, Ala27, Glu28, Gly36, Val37, Tyr39, Val40, and Gly47 from α-Syn, which form the hydrophobic core of the heterodimer (Figure S10). This results in strong binding associated with binding free energy, $\Delta G = -48.26 \pm 9.74$ kcal/mol, as obtained by using the MM-PBSA method averaged over five trajectories.

To confirm whether selected residues are strongly interacting at the interface and are not just close due to the accidental proximity, we also calculated the binding free energies per residue (Table 3) using the most representative structure of the

Table 3. Residues in the α-Syn−Aβ42 Heterodimer Model That Interact Strongly (Binding Free Energy <−2 kcal/mol)

strongly interacting residues			
α-Syn		Aβ42	
Res	dG	Res	dG
VAL 37	−5.37	ILE 32	−8.29
VAL 26	−4.22	PHE 20	−7.12
TYR 39	−3.74	PHE 19	−7.11
ALA 27	−3.66	ILE 31	−4.52
THR 33	−3.22	VAL 18	−3.96
GLU 28	−2.68	VAL 12	−3.86
ALA 30	−2.68	VAL 36	−3.82
LYS 45	−2.61	GLY 38	−3.58
GLN 62	−2.22	LEU 17	−3.31
ALA 29	−2.05	LYS 28	−3.16
		ALA 21	−2.8
		ARG 5	−2.3
		GLN 15	−2.17

heterodimer in the HawkDock server.[66] The performed analysis shows that residues from Aβ42 interact stronger than the ones from α-Syn and there is an overall good agreement between the distance prediction from the trajectory and the energy prediction from the representative model of the residues involved at the interaction interface. It can be seen that residues, which are involved in interaction with partner molecule, are characterized by much lower conformational flexibility than surrounding residues (Figure S12), which confirms that binding stabilizes the interacting regions of both molecules.

3.2.3. Comparison of Aβ42 and α-Syn Homo- and Heterodimer Binding Affinities. A comparison of the predicted binding free energies for representative structures of the heterodimer to those of Aβ42 dimeric models from previous studies (Table 4) indicates that heterodimers are more stable than the respective homodimers. At the same time, interactions between dimeric α-Syn are even stronger. The same relation is showed by a much faster analysis of single representative snapshots, performed by HawkDock (Table 4). It should be noted that relative values, rather than absolute ones, should be compared when molecular modeling methods are used. This result is in agreement with the experimental observation that monomeric α-Syn, contrary to fibrillar forms, inhibits secondary nucleation of Aβ42 fibrils by the formation of strong interactions

Table 4. Binding Free Energies [kcal/mol] Predicted by Using the MM-PBSA (MM) Analysis for the Trajectories with Standard Deviations and the HawkDock (Hawk) Server for Representative Models

	Aβ42 dimer		α-Syn−Aβ42		α-Syn dimer	
	MM	Hawk	MM	Hawk	MM	Hawk
1	−9.90 ± 5.22	−43.38	−48.26 ± 9.74	−113.15	−61.78 ± 35.73	−176.54
2	−22.60 ± 3.80	−52.07			−80.53 ± 13.96	−176.46
3	−20.11 ± 7.01	−58.17			−28.09 ± 12.27	−80.97

between molecules.[32] This allows us to propose with confidence the most probable heterodimer structure, which is shown in Figure 7 (the PDB structure is provided as Supporting Information to the article).
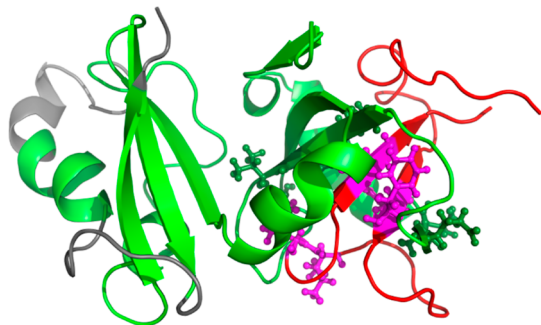
Figure 7. Cartoon representation of the most probable heterodimer complex determined from all-atom implicit MD simulations followed by explicit solvent MD simulation with residues forming stable interactions represented by ball-and-stick representation. In addition, highly flexible fragments are marked with gray color.

Numerous studies have demonstrated that certain amino acid residues or fragments of the Aβ structure play a crucial role in its propensity to form aggregates. Maity and colleagues[96] have shown that Aβ(14−23) forms a hairpin, which, upon aggregation, resembles full-size Aβ42 fibrils. This effect is further observed by Sun et al. as a key factor in the formation of beta-barrels in the early stages of aggregation in AD.[97] In another study, Khaled et al.[98] found that residues 15−20 in Aβ may form contacts, especially in truncated variants lacking C-termini [e.g., Aβ(1−28)]. However, in full-length Aβ42, the key to fibrillization lies in the hydrophobic interactions between the central hydrophobic core (residues 16−22) and the C-terminal region (residues 30−42). Other regions (1−15 and 21−28) lack stable secondary structures and primarily serve as hinges. This finding is corroborated by the work of Itoh et al.,[99] who demonstrated that the formation of two antiparallel beta-sheets between the C-terminus and the center of the peptide is crucial for aggregate formation. The formation of a beta-hairpin also plays a crucial role in dimerization and higher oligomerization of Aβ(29−42) variants, indicating the important role of the C-terminal part of Aβ42.[100,101] The fact that the β-hairpin promotes aggregation is also consistent with the N*-theory showing that the faster the fibril formation, the higher the propensity of the fibril-prone structure.[91,92,95] However, this interaction is not purely hydrophobic, as Arg5 electrostatically stabilizes the molecule, forming interactions with residues such as E22 and K28.[99] This effect was also observed in MD simulations by Huy et al.,[60] showing that Arg5 forms salt bridges with Asp1, Glu22, and Asp23, stabilizing the N-terminal region of Aβ42, which can be disrupted in the presence of copper ions.

Our MD simulations of a heterodimer show that Aβ42 fragments 16−19 and 29−34 (Table S6) are the most involved in forming interactions with α-Syn, which quite accurately fit within the hairpin regions in Aβ42 peptides and oligomers, as shown by other studies.[98,99] They also agree with DMD-predicted regions as hotspots for the α-Syn−Aβ42 interaction, which cover residues 31−60 (the second half of the N-terminal domain) and 61−95 (NAC domain), and residues 10−21 and 31−42 in α-Syn and Aβ42, respectively.[102] Therefore, hydrophobic interactions are also important for the formation of an α-Syn−Aβ42 heterodimer. There are residue ranges for beta-structures in a heterodimer (Figure S8), similar to the Aβ42 homodimers; however, we did not find Arg5 to be important in the formation of contacts with α-Syn. It should be noted that although Chau and Kim found that α-Syn monomers and oligomers promote oligomerization of Aβ42 most likely through binding or coassembly, various parts of Aβ42 are involved in interactions with α-Syn, strongly depending on their conformations.[103]

4. CONCLUSIONS

In this study, we pursued two primary objectives: (i) investigating the interactions between intrinsically disordered monomeric α-Syn and Aβ42 and (ii) assessing the capabilities of implicit solvent simulations in modeling monomeric and heterodimeric systems with disordered characteristics. To achieve this, extensive implicit solvent MD simulations were conducted for both α-Syn and Aβ42, along with their complex, and the results were compared with explicit solvent simulations. Our analysis revealed that the selected all-atom force field with an implicit solvent model (AMBER ff14SBonlysc with the GB-Neck2 model) tended to generate overly compact and ordered structures, particularly noticeable in the case of monomeric α-Syn. However, for the α-Syn−Aβ42 heterodimer, the most probable structure remained stable in both implicit and explicit solvent simulations using AMBER-FB15 and CHARMM36m force fields.

To identify the most stable heterodimer, we conducted a thorough analysis of relevant properties for both monomeric and heteromeric structures. Our findings indicated that the binding of molecules significantly influences their mobility and flexibility. Notably, α-Syn exerts a greater impact on the conformation of Aβ42 than vice versa, attributed to the hydrophobic nature of interchain interactions. Emphasizing the critical role of water models in modeling protein aggregation, we highlighted that the impact of Aβ42 on the aggregation propensity of α-Syn is accurately captured by explicit water models but not by implicit ones. Further research is required to investigate whether this conclusion holds for other scenarios. Comparing the representative α-Syn−Aβ42 heterodimer with Aβ42 and α-Syn homodimer models revealed that it binds approximately two times stronger than Aβ42 dimeric structures but weaker than the α-Syn homodimer. This suggests that α-Syn and Aβ42 can indeed form stable complexes, potentially serving

as seeds for fibril structures and competing with the Aβ42 aggregation process. Our MD simulations of the α-Syn−Aβ42 heterodimer reveal that Aβ42 fragments 16−19 and 29−34 are the most involved in forming interactions with α-Syn, aligning with the β-hairpin regions in Aβ42 peptides and oligomers identified in previous studies.[100,101] These findings also agree with DMD-predicted hotspots for the α-Syn−Aβ42 interaction, covering residues 31−60 and 61−95 in α-Syn and residues 10−21 and 31−42 in Aβ42.

Additionally, we demonstrated the efficiency of using single representative structures for estimating the binding interface and energies, providing results consistent with the more computationally expensive MM-PBSA method across multiple trajectories. Finally, we share the PDB structure of the most probable α-Syn−Aβ42 heterodimer, which can be used to further examine the structure and dynamics and design potential inhibitors.

■ ASSOCIATED CONTENT

ⓈⒾ Supporting Information

The Supporting Information is available free of charge at https://pubs.acs.org/doi/10.1021/acs.jpcb.4c00503.

> Details of the simulations, temperatures used in REMD, fibril-prone Aβ and α-Syn structures data, interacting residues during REMD simulation, rmsd to experimental structures for α-Syn and Aβ42, free energy maps for α-Syn and Aβ42, RMSF of α-Syn and Aβ42 as monomers and in the heterodimer, differences of SASA values upon binding for α-Syn and Aβ42, secondary structure per residue for α-Syn and Aβ42 in implicit and explicit solvent simulations, time evolution of intermolecular contacts between α-Syn and Aβ42, contact maps of α-Syn and Aβ42 and their intermolecular contacts, rmsd and R_g of α-Syn and Aβ42 and the heterodimer during explicit solvent simulations of the α-Syn and Aβ42, and contact map from explicit solvent simulation (PDF)
> PDB structure of the most stable heterodimer (PDB)
> Initial and final protein conformations (ZIP)

■ AUTHOR INFORMATION

Corresponding Author

Paweł Krupa − *Institute of Physics Polish Academy of Sciences, 02-668 Warsaw, Poland;* ⦿ orcid.org/0000-0002-9710-7837; Email: pkrupa@ifpan.edu.pl

Authors

Yuliia Varenyk − *Institute of Physics Polish Academy of Sciences, 02-668 Warsaw, Poland; Department of Theoretical Chemistry, University of Vienna, Vienna 1090, Austria;* ⦿ orcid.org/0009-0009-0536-9345

Panagiotis E. Theodorakis − *Institute of Physics Polish Academy of Sciences, 02-668 Warsaw, Poland;* ⦿ orcid.org/0000-0002-0433-9461

Dinh Q. H. Pham − *Institute of Physics Polish Academy of Sciences, 02-668 Warsaw, Poland*

Mai Suan Li − *Institute of Physics Polish Academy of Sciences, 02-668 Warsaw, Poland;* ⦿ orcid.org/0000-0001-7021-7916

Complete contact information is available at:
https://pubs.acs.org/10.1021/acs.jpcb.4c00503

Notes

The authors declare no competing financial interest.

■ REFERENCES

(1) McKeith, I. G.; Galasko, D.; Kosaka, K.; Perry, E. K.; Dickson, D. W.; Hansen, L. A.; Salmon, D. P.; Lowe, J.; Mirra, S. S.; Byrne, E. J.; et al. Consensus guidelines for the clinical and pahtologic diagnosis of dementia with Lewy bodies (DLB): report of the consortium on DLB international workshop. *Neurology* **1996**, *47*, 1113−1124.

(2) Bachhuber, T.; Katzmarski, N.; McCarter, J. F.; Loreth, D.; Tahirovic, S.; Kamp, F.; Abou-Ajram, C.; Nuscher, B.; Serrano-Pozo, A.; Müller, A.; et al. Inhibition of amyloid-β plaque formation by α-synuclein. *Nat. Med.* **2015**, *21*, 802−807.

(3) Hamilton, R. L. Lewy bodies in Alzheimer's disease: a neuropathological review of 145 cases using α-synuclein immunohistochemistry. *Brain Pathol.* **2000**, *10*, 378−384.

(4) Kosaka, K.; Yoshimura, M.; Ikeda, K.; Budka, H. Diffuse type of Lewy body disease: progressive dementia with abundant cortical Lewy bodies and semile changes of varying degree — a new disease? *Clin. Neuropathol.* **1984**, *3*, 185−192.

(5) Gibb, W.; Esiri, M.; Lees, A. Clinical and pathological features of diffuse cortical Lewy body disease (Lewy body dementia). *Brain* **1987**, *110*, 1131−1153.

(6) Gibb, W.; Luthert, P.; Janota, I.; Lantos, P. Cortical Lewy body dementia: clinical features and classification. *J. Neurol., Neurosurg. Psychiatry* **1989**, *52*, 185−192.

(7) Perry, R.; Irving, D.; Blessed, G.; Fairbairn, A.; Perry, E. Senile dementia of Lewy body type. *J. Neurol. Sci.* **1990**, *95*, 119−139.

(8) Jensen, P.; Sorensen, E.; Petersen, T.; Gliemann, J.; Rasmussen, L. Residues in the synuclein consensus motif of the α-synuclein fragment, NAC, participate in transglutaminase-catalysed cross-linking to Alzheimer-disease amyloid βA4 peptide. *Biochem. J.* **1995**, *310*, 91−94.

(9) Jensen, P.; Hojrup, P.; Hager, H.; Nielsen, M.; Jacobsen, L.; Olesen, O. F.; Gliemann, J.; Jakes, R. Binding of Aβ to alpha- and β-synucleins: identification of segments in α-synuclein/NAC precursor that bind Aβ and NAC. *Biochem. J.* **1997**, *323*, 539−546.

(10) Tsigelny, I. F.; Crews, L.; Desplats, P.; Shaked, G. M.; Sharikov, Y.; Mizuno, H.; Spencer, B.; Rockenstein, E.; Trejo, M.; Platoshyn, O.; et al. Mechanisms of hybrid oligomer formation in the pathogenesis of combined Alzheimer's and Parkinson's diseases. *PLoS One* **2008**, *3*, No. e3135.

(11) Mandal, P. K.; Pettegrew, J. W.; Masliah, E.; Hamilton, R. L.; Mandal, R. Interaction between Aβ Peptide and α Synuclein: Molecular Mechanisms in Overlapping Pathology of Alzheimer's and Parkinson's in Dementia with Lewy Body Disease. *Neurochem. Res.* **2006**, *31*, 1153−1162.

(12) Ivanova, M. I.; Lin, Y.; Lee, Y.-H.; Zheng, J.; Ramamoorthy, A. Biophysical processes underlying cross-seeding in amyloid aggregation and implications in amyloid pathology. *Biophys. Chem.* **2021**, *269*, 106507.

(13) Poma, A. B.; Guzman, H. V.; Li, M. S.; Theodorakis, P. E. Mechanical and thermodynamic properties of Aβ$_{42}$, Aβ$_{40}$, and α-synuclein fibrils: a coarse-grained method to complement experimental studies. *Beilstein J. Nanotechnol.* **2019**, *10*, 500−513.

(14) Bisaglia, M.; Trolio, A.; Bellanda, M.; Bergantino, E.; Bubacco, L.; Mammi, S. Structure and topology of the non-amyloid-β component fragment of human α-synuclein bound to micelles: Implications for the aggregation process. *Protein Sci.* **2006**, *15*, 1408−1416.

(15) Lee, J.; Choi, C.; Lee, S. Membrane-bound α-Synuclein Has a High Aggregation Propensity and the Ability to Seed the Aggregation of the Cytosolic Form. *J. Biol. Chem.* **2002**, *277*, 671−678.

(16) Benilova, I.; Karran, E.; De Strooper, B. The toxic Aβ oligomer and Alzheimer's disease: an emperor in need of clothes. *Nat. Neurosci.* **2012**, *15*, 349−357.

(17) Ingelsson, M. Alpha-synuclein oligomers-neurotoxic molecules in Parkinson's disease and other lewy body disorders. *Front. Neurosci.* **2016**, *10*, 408.

(18) Huang, Y.-r.; Liu, R.-t. The Toxicity and Polymorphism of β-Amyloid Oligomers. *Int. J. Mol. Sci.* **2020**, *21*, 4477.

(19) Masters, C.; Simms, G.; Weinman, N. A.; Multhaup, G.; McDonald, B.; Beyreuther, K. Amyloid plaque core protein in Alzheimer disease and Down syndrome. *Proc. Natl. Acad. Sci. U.S.A.* **1985**, *82*, 4245−4249.

(20) Boopathi, S.; Dinh Quoc Huy, P.; Gonzalez, W.; Theodorakis, P. E.; Li, M. S. Zinc binding promotes greater hydrophobicity in Alzheimer's Aβ42 peptide than copper binding: Molecular dynamics and solvation thermodynamics studies. *Proteins: Struct., Funct., Bioinf.* **2020**, *88*, 1285−1302.

(21) Selkoe, D. Translating cell biology into therapeutic advances in Alzheimer's disease. *Nature* **1999**, *399*, A23−A31.

(22) Jarrett, J.; Berger, E.; Lansbury, P. T. The carboxy terminus of the .beta. amyloid protein is critical for the seeding of amyloid formation: Implications for the pathogenesis of Alzheimer's disease. *Biochemistry* **1993**, *32*, 4693−4697.

(23) Dickson, D. The pathogenesis of senile plaques. *J. Neuropathol. Exp. Neurol.* **1997**, *56*, 321−339.

(24) Masliah, E.; Rockenstein, E.; Veinbergs, I.; Sagara, Y.; Mallory, M.; Hashimoto, M.; Mucke, L. β-Amyloid peptides enhance α-synuclein accumulation and neuronal deficits in a transgenic mouse model linking Alzheimer's disease and Parkinson's disease. *Proc. Natl. Acad. Sci. U.S.A.* **2001**, *98*, 12245−12250.

(25) Serpell, L. C. Alzheimer's amyloid fibrils: structure and assembly. *Biochim. Biophys. Acta, Mol. Basis Dis.* **2000**, *1502*, 16−30.

(26) Kirkitadze, M. D.; Condron, M. M.; Teplow, D. B. Identification and characterization of key kinetic intermediates in amyloid β-protein fibrillogenesis11Edited by F. Cohen. *J. Mol. Biol.* **2001**, *312*, 1103−1119.

(27) Bernstein, S. L.; Dupuis, N. F.; Lazo, N. D.; Wyttenbach, T.; Condron, M. M.; Bitan, G.; Teplow, D. B.; Shea, J.-E.; Ruotolo, B. T.; Robinson, C. V.; et al. Amyloid-β protein oligomerization and the importance of tetramers and dodecamers in the aetiology of Alzheimer's disease. *Nat. Chem.* **2009**, *1*, 326−331.

(28) Lashuel, H.; Overk, C.; Oueslati, A.; Masliah, E. The many faces of α-synuclein: from structure and toxicity to therapeutic target. *Nat. Rev. Neurosci.* **2013**, *14*, 38−48.

(29) Yokota, O.; Terada, S.; Ishizu, H.; Ujike, H.; Ishihara, T.; Nakashima, H.; Yasuda, M.; Kitamura, Y.; Ueda, K.; Checler, F.; et al. NACP/α-Synuclein, NAC, and β-amyloid pathology of familial Alzheimer's disease with the E184D presenilin-1 mutation: a clinicopathological study of two autopsy cases. *Acta Neuropathol.* **2002**, *104*, 637−648.

(30) Liu, C.; Giasson, B.; Lewis, K.; Lee, V.; DeMartino, G.; Thomas, P. A Precipitating Role for Truncated α-Synuclein and the Proteasome in α-Synuclein Aggregation. *J. Biol. Chem.* **2005**, *280*, 22670−22678.

(31) Köppen, J.; Schulze, A.; Machner, L.; Wermann, M.; Eichentopf, R.; Guthardt, M.; Hähnel, A.; Klehm, J.; Kriegeskorte, M.-C.; Hartlage-Rübsamen, M.; et al. Amyloid-Beta Peptides Trigger Aggregation of Alpha-Synuclein In Vitro. *Molecules* **2020**, *25*, 580.

(32) Chia, S.; Flagmeier, P.; Habchi, J.; Lattanzi, V.; Linse, S.; Dobson, C. M.; Knowles, T. P. J.; Vendruscolo, M. Monomeric and fibrillar α-synuclein exert opposite effects on the catalytic cycle that promotes the proliferation of Aβ42 aggregates. *Proc. Natl. Acad. Sci. U.S.A.* **2017**, *114*, 8005−8010.

(33) Jumper, J.; Evans, R.; Pritzel, A.; Green, T.; Figurnov, M.; Ronneberger, O.; Tunyasuvunakool, K.; Bates, R.; Žídek, A.; Potapenko, A.; et al. Highly accurate protein structure prediction with AlphaFold. *Nature* **2021**, *596*, 583−589.

(34) Evans, R.; O'Neill, M.; Pritzel, A.; Antropova, N.; Senior, A.; Green, T.; Žídek, A.; Bates, R.; Blackwell, S.; Yim, J.; et al. Protein complex prediction with AlphaFold-Multimer. *bioRxiv*, **2022**. https://www.biorxiv.org/content/early/2022/03/10/2021.10.04.463034 accessed: 2024−04−09

(35) Liu, J.; Guo, Z.; Wu, T.; Roy, R. S.; Quadir, F.; Chen, C.; Cheng, J. Enhancing alphafold-multimer-based protein complex structure prediction with MULTICOM in CASP15. *Commun. Biol.* **2023**, *6*, 1140.

(36) Hansmann, U. Parallel tempering algorithm for conformational studies of biological molecules. *Chem. Phys. Lett.* **1997**, *281*, 140−150.

(37) Sugita, Y.; Okamoto, Y. Replica-exchange molecular dynamics method for protein folding. *Chem. Phys. Lett.* **1999**, *314*, 141−151.

(38) Götz, A. W.; Williamson, M. J.; Xu, D.; Poole, D.; Le Grand, S.; Walker, R. C. Routine Microsecond Molecular Dynamics Simulations with AMBER on GPUs. 1. Generalized Born. *J. Chem. Theory Comput.* **2012**, *8*, 1542−1555.

(39) Harris, R. C.; Shen, J. GPU-Accelerated Implementation of Continuous Constant pH Molecular Dynamics in Amber: pKa Predictions with Single-pH Simulations. *J. Chem. Inf. Model.* **2019**, *59*, 4821−4832.

(40) Lee, T.-S.; Cerutti, D. S.; Mermelstein, D.; Lin, C.; LeGrand, S.; Giese, T. J.; Roitberg, A.; Case, D. A.; Walker, R. C.; York, D. M. GPU-Accelerated Molecular Dynamics and Free Energy Methods in Amber18: Performance Enhancements and New Features. *J. Chem. Inf. Model.* **2018**, *58*, 2043−2050.

(41) Kmiecik, S.; Gront, D.; Kolinski, M.; Wieteska, L.; Dawid, A. E.; Kolinski, A. Coarse-Grained Protein Models and Their Applications. *Chem. Rev.* **2016**, *116*, 7898−7936.

(42) Tomasi, J.; Persico, M. Molecular Interactions in Solution: An Overview of Methods Based on Continuous Distributions of the Solvent. *Chem. Rev.* **1994**, *94*, 2027−2094.

(43) Lang, E. J. M.; Baker, E. G.; Woolfson, D. N.; Mulholland, A. J. Generalized Born Implicit Solvent Models Do Not Reproduce Secondary Structures of De Novo Designed Glu/Lys Peptides. *J. Chem. Theory Comput.* **2022**, *18*, 4070−4076.

(44) Nguyen, P. H.; Li, M. S.; Derreumaux, P. Effects of all-atom force fields on amyloid oligomerization: replica exchange molecular dynamics simulations of the Aβ16−22 dimer and trimer. *Phys. Chem. Chem. Phys.* **2011**, *13*, 9778.

(45) Shao, Q.; Zhu, W. Assessing AMBER force fields for protein folding in an implicit solvent. *Phys. Chem. Chem. Phys.* **2018**, *20*, 7206−7216.

(46) Huang, J.; Rauscher, S.; Nawrocki, G.; Ran, T.; Feig, M.; de Groot, B. L.; Grubmüller, H.; MacKerell, A. D. CHARMM36m: an improved force field for folded and intrinsically disordered proteins. *Nat. Methods* **2017**, *14*, 71−73.

(47) Yang, M.; Teplow, D. B. Amyloid β-Protein Monomer Folding: Free-Energy Surfaces Reveal Alloform-Specific Differences. *J. Mol. Biol.* **2008**, *384*, 450−464.

(48) Krupa, P.; Karczyńska, A. S.; Mozolewska, M. A.; Liwo, A.; Czaplewski, C. UNRES-Dock—protein−protein and peptide−protein docking by coarse-grained replica-exchange MD simulations. *Bioinformatics* **2021**, *37*, 1613−1615.

(49) Nguyen, H.; Maier, J.; Huang, H.; Perrone, V.; Simmerling, C. Folding simulations for proteins with diverse topologies are accessible in days with a physics-based force field and implicit solvent. *J. Am. Chem. Soc.* **2014**, *136*, 13959−13962.

(50) Case, D.; Cerutti, D. T. E.; Cheatham, I.; Darden, T.; Duke, R.; Giese, T.; Gohlke, H.; Goetz, A.; Greene, D.; Homeyer, N.; et al. *Amber 2022*, 2022.

(51) Krupa, P.; Quoc Huy, P. D.; Li, M. S. Properties of monomeric Aβ42 probed by different sampling methods and force fields: Role of energy components. *J. Chem. Phys.* **2019**, *151*, 055101.

(52) Man, V. H.; He, X.; Derreumaux, P.; Ji, B.; Xie, X. Q.; Nguyen, P. H.; Wang, J. Effects of All-Atom Molecular Mechanics Force Fields on Amyloid Peptide Assembly: The Case of Aβ$_{16-22}$ Dimer. *J. Chem. Theory Comput.* **2019**, *15*, 1440–1452.

(53) Patriksson, A.; van der Spoel, D. A temperature predictor for parallel tempering simulations. *Phys. Chem. Chem. Phys.* **2008**, *10*, 2073–2077.

(54) Essmann, U.; Perera, L.; Berkowitz, M. L.; Darden, T.; Lee, H.; Pedersen, L. G. A smooth particle mesh Ewald method. *J. Chem. Phys.* **1995**, *103*, 8577–8593.

(55) Wang, L. P.; McKiernan, K. A.; Gomes, J.; Beauchamp, K. A.; Head-Gordon, T.; Rice, J. E.; Swope, W. C.; Martínez, T. J.; Pande, V. S. Building a More Predictive Protein Force Field: A Systematic and Reproducible Route to AMBER-FB15. *J. Phys. Chem. B* **2017**, *121*, 4023–4039.

(56) Best, R. B.; Zhu, X.; Shim, J.; Lopes, P. E. M.; Mittal, J.; Feig, M.; MacKerell, A. D. J. Optimization of the Additive CHARMM All-Atom Protein Force Field Targeting Improved Sampling of the Backbone ϕ, ψ and Side-Chain χ1 and χ2 Dihedral Angles. *J. Chem. Theory Comput.* **2012**, *8*, 3257–3273.

(57) Reid, L. M.; Guzzetti, I.; Svensson, T.; Carlsson, A.-C.; Su, W.; Leek, T.; von Sydow, L.; Czechtizky, W.; Miljak, M.; Verma, C.; et al. How well does molecular simulation reproduce environment-specific conformations of the intrinsically disordered peptides PLP, TP2 and ONEG? *Chem. Sci.* **2022**, *13*, 1957–1971.

(58) Jo, S.; Kim, T.; Iyer, V. G.; Im, W. CHARMM-GUI: A web-based graphical user interface for CHARMM. *J. Comput. Chem.* **2008**, *29*, 1859–1865.

(59) Wang, L.-P.; Martinez, T. J.; Pande, V. S. Building Force Fields: An Automatic, Systematic, and Reproducible Approach. *J. Phys. Chem. Lett.* **2014**, *5*, 1885–1891.

(60) Huy, P. D. Q.; Vuong, Q. V.; La Penna, G.; Faller, P.; Li, M. S. Impact of Cu(II) Binding on Structures and Dynamics of Aβ$_{42}$ Monomer and Dimer: Molecular Dynamics Study. *ACS Chem. Neurosci.* **2016**, *7*, 1348–1363.

(61) Zhang, Y.; Hashemi, M.; Lv, Z.; Williams, B.; Popov, K. I.; Dokholyan, N. V.; Lyubchenko, Y. L. High-speed atomic force microscopy reveals structural dynamics of α -synuclein monomers and dimers. *J. Chem. Phys.* **2018**, *148*, 123322.

(62) Kabsch, W.; Sander, C. Dictionary of protein secondary structure: Pattern recognition of hydrogen-bonded and geometrical features. *Biopolymers* **1983**, *22*, 2577–2637.

(63) Weiser, J.; Shenkin, P. S.; Still, W. C. Approximate atomic surfaces from linear combinations of pairwise overlaps (LCPO). *J. Comput. Chem.* **1999**, *20*, 217–230.

(64) Krupa, P.; Sieradzan, A. K.; Mozolewska, M. A.; Li, H.; Liwo, A.; Scheraga, H. A. Dynamics of Disulfide-Bond Disruption and Formation in the Thermal Unfolding of Ribonuclease A. *J. Chem. Theory Comput.* **2017**, *13*, 5721–5730.

(65) Genheden, S.; Ryde, U. The MM/PBSA and MM/GBSA methods to estimate ligand-binding affinities. *Expert Opin. Drug Discovery* **2015**, *10*, 449–461.

(66) Weng, G.; Wang, E.; Wang, Z.; Liu, H.; Zhu, F.; Li, D.; Hou, T. HawkDock: a web server to predict and analyze the protein-protein complex based on computational docking and MM/GBSA. *Nucleic Acids Res.* **2019**, *47*, W322–W330.

(67) Krupa, P.; Spodzieja, M.; Sieradzan, A. K. Prediction of CD28-CD86 protein complex structure using different level of resolution approach. *J. Mol. Graphics Modell.* **2021**, *103*, 107802.

(68) Uversky, V. N.; Li, J.; Fink, A. L. Metal-triggered structural transformations, aggregation, and fibrillation of human α-synuclein: A possible molecular link between parkinson's disease and heavy metal exposure. *J. Biol. Chem.* **2001**, *276*, 44284–44296.

(69) Bernstein, S. L.; Liu, D.; Wyttenbach, T.; Bowers, M. T.; Lee, J. C.; Gray, H. B.; Winkler, J. R. α-Synuclein: Stable compact and extended monomeric structures and pH dependence of dimer formation. *J. Am. Soc. Mass Spectrom.* **2004**, *15*, 1435–1443.

(70) Bitan, G.; Kirkitadze, M. D.; Lomakin, A.; Vollers, S. S.; Benedek, G. B.; Teplow, D. B. Amyloid β-protein (Aβ) assembly: Aβ40 and Aβ42

oligomerize through distinct pathways. *Proc. Natl. Acad. Sci. U.S.A.* **2003**, *100*, 330–335.

(71) Festa, G.; Mallamace, F.; Sancesario, G. M.; Corsaro, C.; Mallamace, D.; Fazio, E.; Arcidiacono, L.; Garcia Sakai, V.; Senesi, R.; Preziosi, E.; et al. Aggregation States of Aβ1–40, Aβ1–42 and Aβp3–42 Amyloid Beta Peptides: A SANS Study. *Int. J. Mol. Sci.* **2019**, *20*, 4126.

(72) Ahmed, M. C.; Skaanning, L. K.; Jussupow, A.; Newcombe, E. A.; Kragelund, B. B.; Camilloni, C.; Langkilde, A. E.; Lindorff-Larsen, K. Refinement of α-Synuclein Ensembles Against SAXS Data: Comparison of Force Fields and Methods. *Front. Mol. Biosci.* **2021**, *8*, 654333.

(73) Gallardo, J.; Escalona-Noguero, C.; Sot, B. Role of α-Synuclein Regions in Nucleation and Elongation of Amyloid Fiber Assembly. *ACS Chem. Neurosci.* **2020**, *11*, 872–879.

(74) Watts, C. R.; Gregory, A. J.; Frisbie, C. P.; Lovas, S. Structural properties of amyloid β(1-40) dimer explored by replica exchange molecular dynamics simulations. *Proteins: Struct., Funct., Bioinf.* **2017**, *85*, 1024–1045.

(75) Duan, S.; Guan, X.; Lin, R.; Liu, X.; Yan, Y.; Lin, R.; Zhang, T.; Chen, X.; Huang, J.; Sun, X.; et al. Silibinin inhibits acetylcholinesterase activity and amyloid β peptide aggregation: a dual-target drug for the treatment of Alzheimer's disease. *Neurobiol. Aging* **2015**, *36*, 1792–1807.

(76) Truong, P. M.; Viet, M. H.; Nguyen, P. H.; Hu, C.-K.; Li, M. S. Effect of Taiwan Mutation (D7H) on Structures of Amyloid-β Peptides: Replica Exchange Molecular Dynamics Study. *J. Phys. Chem. B* **2014**, *118*, 8972–8981.

(77) Ono, K.; Condron, M. M.; Teplow, D. B. Structure–neurotoxicity relationships of amyloid β-protein oligomers. *Proc. Natl. Acad. Sci. U.S.A.* **2009**, *106*, 14745–14750.

(78) Carballo-Pacheco, M.; Strodel, B. Comparison of force fields for Alzheimer's A: A case study for intrinsically disordered proteins. *Protein Sci.* **2017**, *26*, 174–185.

(79) Rosenman, D. J.; Wang, C.; García, A. E. Characterization of Aβ Monomers through the Convergence of Ensemble Properties among Simulations with Multiple Force Fields. *J. Phys. Chem. B* **2016**, *120*, 259–277.

(80) Lin, Y.-S.; Pande, V. S. Effects of Familial Mutations on the Monomer Structure of Aβ42. *Biophys. J.* **2012**, *103*, L47–L49.

(81) Rosenman, D. J.; Connors, C. R.; Chen, W.; Wang, C.; García, A. E. Aβ Monomers Transiently Sample Oligomer and Fibril-Like Configurations: Ensemble Characterization Using a Combined MD/NMR Approach. *J. Mol. Biol.* **2013**, *425*, 3338–3359.

(82) Nasica-Labouze, J.; Nguyen, P. H.; Sterpone, F.; Berthoumieu, O.; Buchete, N. V.; Coté, S.; De Simone, A.; Doig, A. J.; Faller, P.; Garcia, A.; et al. Amyloid β Protein and Alzheimer's Disease: When Computer Simulations Complement Experimental Studies. *Chem. Rev.* **2015**, *115*, 3518–3563.

(83) Meade, R. M.; Fairlie, D. P.; Mason, J. M. Alpha-synuclein structure and Parkinson's disease - Lessons and emerging principles. *Mol. Neurodegener.* **2019**, *14*, 29.

(84) Zhang, Y.; Wang, Y.; Liu, Y.; Wei, G.; Ding, F.; Sun, Y. Molecular Insights into the Misfolding and Dimerization Dynamics of the Full-Length α-Synuclein from Atomistic Discrete Molecular Dynamics Simulations. *ACS Chem. Neurosci.* **2022**, *13*, 3126–3137.

(85) Wang, C.; Zhao, C.; Li, D.; Tian, Z.; Lai, Y.; Diao, J.; Liu, C. Versatile structures of α-synuclein. *Front. Mol. Neurosci.* **2016**, *9*, 48.

(86) Rodriguez, J. A.; Ivanova, M. I.; Sawaya, M. R.; Cascio, D.; Reyes, F. E.; Shi, D.; Sangwan, S.; Guenther, E. L.; Johnson, L. M.; Zhang, M.; et al. Structure of the toxic core of α-synuclein from invisible crystals. *Nature* **2015**, *525*, 486–490.

(87) Ambroso, M. R.; Haworth, I. S.; Langen, R. Structural Characterization of Membrane-Curving Proteins: Site-Directed Spin Labeling, EPR, and Computational Refinement. *Methods Enzymol.* **2015**, *564*, 259–288.

(88) Dettmer, U.; Newman, A. J.; Soldner, F.; Luth, E. S.; Kim, N. C.; Von Saucken, V. E.; Sanderson, J. B.; Jaenisch, R.; Bartels, T.; Selkoe, D. Parkinson-causing α-synuclein missense mutations shift native

tetramers to monomers as a mechanism for disease initiation. *Nat. Commun.* **2015**, *6*, 7314.

(89) Kim, D.-H.; Lee, J.; Mok, K. H.; Lee, J. H.; Han, K.-H. Salient Features of Monomeric Alpha-Synuclein Revealed by NMR Spectroscopy. *Biomolecules* **2020**, *10*, 428.

(90) Yu, H.; Han, W.; Ma, W.; Schulten, K. Transient β-hairpin formation in α-synuclein monomer revealed by coarse-grained molecular dynamics simulation. *J. Chem. Phys.* **2015**, *143*, 243142.

(91) Li, M. S.; Co, N. T.; Reddy, G.; Hu, C.-K.; Straub, J. E.; Thirumalai, D. Factors Governing Fibrillogenesis of Polypeptide Chains Revealed by Lattice Models. *Phys. Rev. Lett.* **2010**, *105*, 218101.

(92) Chakraborty, D.; Straub, J. E.; Thirumalai, D. Differences in the free energies between the excited states of Aβ40 and Aβ42 monomers encode their aggregation propensities. *Proceedings of the National Academy of Sciences*, 2020; Vol. 117, pp 19926−19937.

(93) Nam, H. B.; Kouza, M.; Zung, H.; Li, M. S. Relationship between population of the fibril-prone conformation in the monomeric state and oligomer formation times of peptides: Insights from all-atom simulations. *J. Chem. Phys.* **2010**, *132*, 165104.

(94) Huang, F.; Wang, Y.; Zhang, Y.; Wang, C.; Lian, J.; Ding, F.; Sun, Y. Dissecting the Self-assembly Dynamics of Imperfect Repeats in α-Synuclein. *J. Chem. Inf. Model.* **2023**, *63*, 3591−3600.

(95) Thu, T. T. M.; Co, N. T.; Tu, L. A.; Li, M. S. Aggregation rate of amyloid beta peptide is controlled by beta-content in monomeric state. *J. Chem. Phys.* **2019**, *150*, 225101.

(96) Maity, S.; Hashemi, M.; Lyubchenko, Y. L. Nano-assembly of amyloid β peptide: role of the hairpin fold. *Sci. Rep.* **2017**, *7*, 2344.

(97) Sun, Y.; Kakinen, A.; Wan, X.; Moriarty, N.; Hunt, C. P.; Li, Y.; Andrikopoulos, N.; Nandakumar, A.; Davis, T. P.; Parish, C. L.; et al. Spontaneous formation of β-sheet nano-barrels during the early aggregation of Alzheimer's amyloid beta. *Nano Today* **2021**, *38*, 101125.

(98) Khaled, M.; Rönnbäck, I.; Ilag, L. L.; Gräslund, A.; Strodel, B.; Österlund, N. A Hairpin Motif in the Amyloid-β Peptide Is Important for Formation of Disease-Related Oligomers. *J. Am. Chem. Soc.* **2023**, *145*, 18340−18354.

(99) Itoh, S. G.; Yagi-Utsumi, M.; Kato, K.; Okumura, H. Key Residue for Aggregation of Amyloid-β Peptides. *ACS Chem. Neurosci.* **2022**, *13*, 3139−3151.

(100) Itoh, S. G.; Okumura, H. Dimerization Process of Amyloid-β(29−42) Studied by the Hamiltonian Replica-Permutation Molecular Dynamics Simulations. *J. Phys. Chem. B* **2014**, *118*, 11428−11436.

(101) Itoh, S. G.; Okumura, H. Oligomer Formation of Amyloid-β(29−42) from Its Monomers Using the Hamiltonian Replica-Permutation Molecular Dynamics Simulation. *J. Phys. Chem. B* **2016**, *120*, 6555−6561.

(102) Huang, F.; Liu, Y.; Wang, Y.; Xu, J.; Lian, J.; Zou, Y.; Wang, C.; Ding, F.; Sun, Y. Co-aggregation of α-synuclein with amyloid-β stabilizes β-sheet-rich oligomers and enhances the formation of β-barrels. *Phys. Chem. Chem. Phys.* **2023**, *25*, 31604−31614.

(103) Chau, E.; Kim, J. R. α-synuclein-assisted oligomerization of β-amyloid (1−42). *Arch. Biochem. Biophys.* **2022**, *717*, 109120.